Exploring the solar-flare predictive potential of non-neutralized currents and Ising energy in solar active regions

I. Kontogiannis[1], M. K. Georgoulis[1], K. Florios[1], S.-H. Park[2] and J. A. Guerra[2]

1. Research center for Astronomy and Applied Mathematics, Academy of Athens, Soranou Efesiou Str. 4 Athens, GR-11527, Greece
2. School of Physics, Trinity College Dublin, Dublin 2, Ireland

Abstract

The immediate effect of solar flares on the geospace environment imposes strict conditions on the efficiency of prediction and requires the development of new methods with increasing sophistication and accuracy. In this context, we investigate the predictive potential of certain solar active-region properties reported in the literature as flare-associated but never widely used in an operational framework. We use Space weather Helioseismic Magnetic Imager Active Region Patch (SHARP) data to calculate the non-neutralized currents and Ising energy of a sizable sample of active regions. These quantities were chosen because a) electric currents supply the free magnetic energy necessary for flaring activity, b) the magnetic complexity, as modeled by the Ising energy, is an indication of potentially intense flaring activity, and c) promising results have been reported in the literature about their potential as flare predictors but no study has been performed on more extended samples. We describe the extraction process of these properties from SHARP data. Preliminary results show that both non-neutralized currents and Ising energy facilitate some distinction between flaring and non-flaring active regions and that there is a tendency for larger flares to occur for larger values of these properties. We finally discuss their efficiency and integrability of these predictors in the operational framework of the FLARECAST project of the European Commission.

Method

Non neutralized current calculations

We follow the method of Georgoulis, Titov & Mikić (2012):

- Input: Vector magnetogram
- The vertical component of the magnetic field is used to produce partitions (Barnes et al. 2005), based on appropriate magnetic flux density, area and enclosed flux thresholds (100 G, 40 pixel, $5\cdot10^{19}$ Mx).
- Ampère's law is used to calculate the total vertical current within each partition: $J_z = \frac{1}{\mu_0}\left(\frac{\partial B_y}{\partial x} - \frac{\partial Bx}{\partial y}\right)$
- The vector of the magnetic field at the photosphere is calculated via a potential field extrapolation (Alissandrakis 1981).
- Ampère's law is used to calculate the corresponding current for the potential field I_{pot}.
- A partition is non-neutralized only if $\boldsymbol{I > 5I_{pot}}$ **and** $\boldsymbol{I > 3\,\delta I}$.

Ising Energy calculations

We follow the procedure proposed by Ahmed et al. 2010.

- Input: LOS magnetogram.
- Low absolute value pixels are eliminated (set to 0).
- *Ising Energy*, E_{Ising} is calculated via the formula: $E = -\sum_{ij}^{N} \frac{S_i S_j}{d^2}$

where, $S = +1$ *(-1)* for a positive (negative) pixel and d the distance between pairs of opposite polarity pixels.

- We also explored, $\boldsymbol{E_{Ising,part}}$ which is calculated for a partitioned magnetogram, for the pairs of opposite polarity partitions.

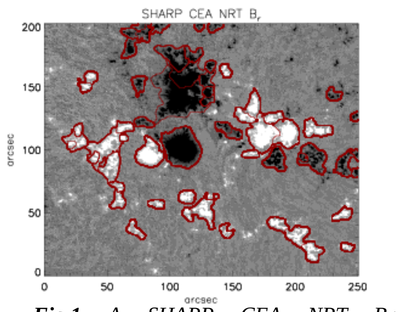

Fig.1 *A SHARP CEA NRT Br magnetogram with overplotted partitions*

Table I. The AR sample

NOAA	t_{start}	t_{end}	B	C	M	X	FI
11072	2010-05-20	2010-05-24	2	0	0	0	0.06
11158	2011-02-10	2011-02-15	1	25	4	1	100.67
11429	2012-03-04	2012-03-10	0	34	12	6	278.15
11515	2012-06-28	2012-07-07	2	39	14	0	53.97
11640	2013-01-01	2013-01-05	5	4	0	0	1.81
11663	2013-01-29	2013-02-03	2	2	0	0	0.55
11748	2013-05-15	2013-05-18	0	10	4	0	31.16
11863	2013-10-10	2013-10-13	0	0	0	0	0.0
11875	2013-10-18	2013-10-28	0	81	18	2	93.60
11882	2013-10-26	2013-10-30	0	7	10	0	49.10
11923	2013-12-12	2013-12-15	0	0	0	0	0.0

Two kinds of SHARP Cylindrical Equal Area (CEA) projected, Near Real Time (NRT) data (Bobra et al. 2014) are used

- A sample of 11 AR time-series (Table I).
- A representative sample of *9454* SHARP CEA NRT cut-outs, for *336* randomly selected days between September 2012 and May 2016, with a 6 h cadence.

The associated flaring activity within a 24 h time window is inferred by the Geostationary Operational Environmental Satellite (GOES) flare catalogue (http://www.swpc.noaa.gov).

Results

Four parameters are tested for their predictive potential:

- **the *total unsigned non-neutralized current*** $I_{NN,tot} = \sum_i \left|I_i^{NN}\right|$
- **the *maximum non-neutralized partition current*** $I_{NN,\max} = \max\{\left|I_i^{NN}\right|\}$
- ***The Ising energy of the original magnetogram, E_{Ising}***
- ***The Ising energy of the partitioned magnetogram, $E_{Ising,part}$***

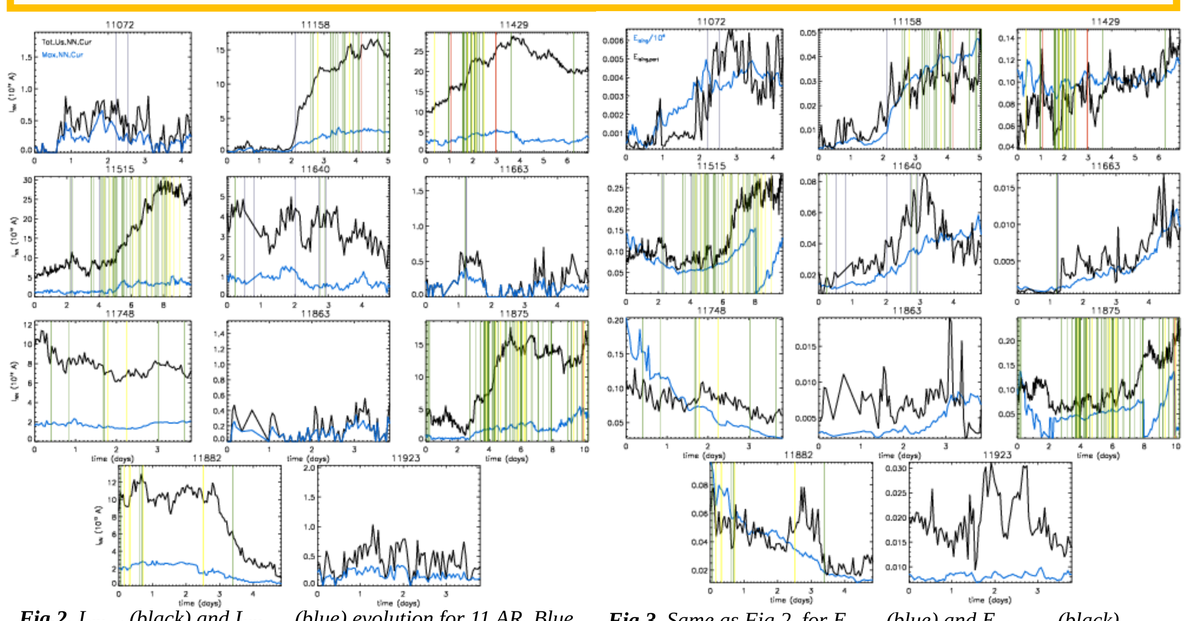

Fig.2. *$I_{NN,tot}$ (black) and $I_{NN,max}$ (blue) evolution for 11 AR. Blue, green, yellow and red lines mark the occurrence times of B-, C-, M- and X-class flares correspondingly.*

Fig.3. *Same as Fig.2, for E_{Ising}, (blue) and $E_{Ising,part}$ (black).*

To test the predictive capability of the four parameters, against that of the total unsigned magnetic flux (provided with the SHARP data) we use Bayesian inference:

$$p = \frac{F+1}{N+2} \qquad \delta p = \sqrt{\frac{p(1-p)}{N+3}}$$

where, N and *F* are the numbers of total flaring AR with a property value higher than a threshold.

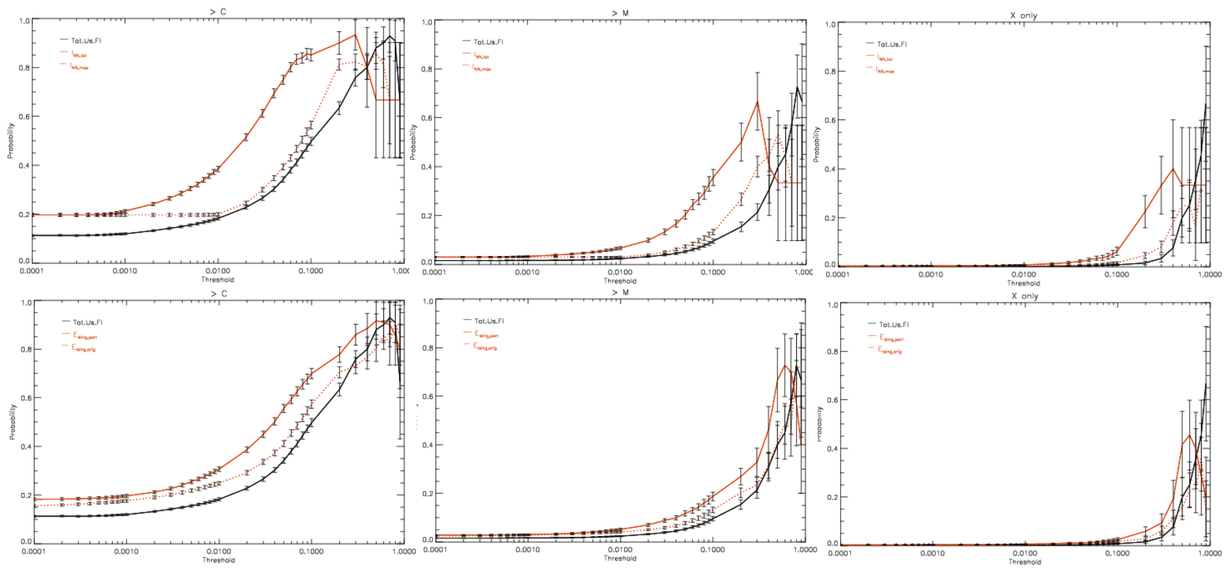

Fig.7. *Top row: Bayesian inferred probabilities for flares stronger than C1.0 (left), M1.0 (middle) and X1.0 (right) for various thresholds of $I_{NN,tot}$ (red solid line) and $I_{NN,max}$ (red dotted line). The black solid line corresponds to the total unsigned magnetic flux. Bottom: Same as top for $E_{Ising,part}$ (solid red line) and E_{Ising} (dotted red line).*

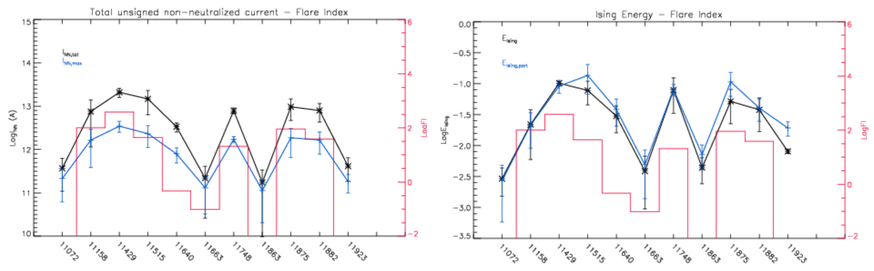

Fig.4. *Left: $I_{NN,tot}$ (black) and $I_{NN,max}$ (blue) time-averaged values and the total flare index over the duration of each AR time-series. Right: the same for E_{ising} (black) and $E_{Ising,part}$ (blue).*

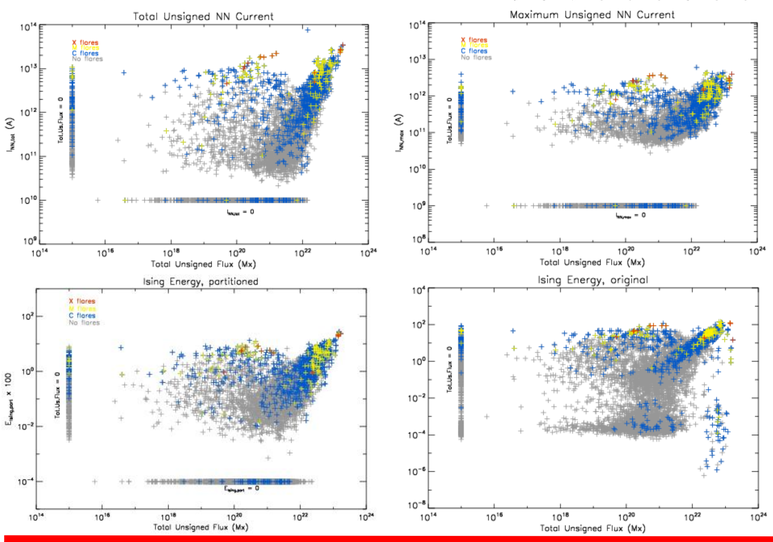

Fig.5. *$I_{NN,tot}$ (left) and $I_{NN,max}$ (right) versus the total unsigned magnetic flux for the representative sample of SHARP CEA NRT data. Blue, yellow and red crosses correspond respectively to data associated with C-, M- and X-class flares within a 24 h time window.*

Fig.6. *Same as Fig.5 for $E_{Ising,part}$ (left) and E_{Ising}, (right).*

Conclusions

- AR with high flare productivity exhibit, on average, higher $I_{NN,tot}$, $I_{NN,max}$, E_{Ising}, $E_{Ising,part}$, by more than an order of magnitude while clear peaks in $I_{NN,tot}$ and $E_{Ising,part}$ are associated either with X-class flares or repeated flaring activity (Fig. 2,3,4).
- $I_{NN,tot}$ and $I_{NN,max}$ also show potential to distinguish between flare-quiet and flare-productive phases of AR evolution (as e.g. AR 11158, 11429, 11882 in Fig. 2).
- The occurrence of strongest flares increases as the values of the four parameters increase while X-class flares are associated only with the highest values (Fig. 5, 6).
- All four parameters show a better predictive potential than the total unsigned magnetic flux (Fig. 7).
- The total unsigned non-neutralized current $I_{NN,tot}$ performs significantly better than the rest of the parameters (Fig. 7, top row).
- Using the partitioned magnetogram to calculate Ising energy ($E_{Ising,part}$) clearly improves the performance of the parameter (Fig. 7, bottom row).
- Both $E_{Ising,part}$ and $I_{NN,tot}$ show high importance when used in neural networks models for forecasting C-, M- and X-class flares, with the Garson (Garson 1991) and Olden (Olden et al. 2004) methods, along-side well studied flaring predictors.

Acknowledgments

This research has been financed by the European Union's Horizon2020 research and innovation programme under grant agreement No.640216 for the "Flare Likelihood And Region Eruption foreCASTing" (Flarecast) project. The data used here are courtesy of NASA/*SDO* and the HMI science team, as well as the Geostationary Satellite System (*GOES*) team.

References

Ahmed, O., Qahwaji, R., Colak, T., et al. 2010, *Vis. Comput.* **26**, 385.
Alissandrakis, C. E. 1981, A&A, 100, 197
Barnes, G., Longcope, D. W., & Leka, K. D. 2005, ApJ, 629, 561
Bobra, M. G., Sun, X., Hoeksema, J. T., et al. 2014, Sol. Phys., 289, 3549
Garson, G.D., 1991, AI Expert, 6, 46
Georgoulis, M.K., Titov, V.S., & Mikić, Z., 2012, ApJ, 761, 61
Olden, J.D., Joy, M.K., & Death, R.G., 2004, Ecol Model, 178, 389